ELSEVIER

Remote Sensing of Environment

Retrieval of Leaf Area Index and Canopy Closure from CASI Data over the BOREAS Flux Tower Sites

Baoxin Hu,[*†] *Kris Inannen,*[*] *and John R. Miller*[*]

This study is to investigate the retrievals of the canopy leaf area index (LAI) and canopy closure using a canopy model. The data used were obtained by the Compact Airborne Spectrographic Imager (CASI) with a spatial resolution of 2 m over the flux tower sites in the BOREAS study area in the winter of 1994 and in the summer of 1996. The FLIM (Forest–Light Interaction Model) was adapted to describe the reflectance properties of the boreal forest canopies investigated by considering the effect of the ellipticity of the conifer crowns on shadows and crown transmittance. The LAI and canopy closure images were produced for the flux tower sites investigated from the CASI winter images using the modified FLIM. Visual evaluation shows that the spatial patterns shown in the canopy LAI and canopy closure images are consistent with those exhibited by the color composite CASI images for the same sites. The canopy LAI images were further validated by field-measured LAI along specific transects. The R^2 between the retrieved canopy LAI and the field-measured LAI ranges from 0.51 to 0.86 for the sites investigated. Furthermore, the CASI summer image over the Old Black Spruce site in the BOREAS souther study area (SOBS) was used to investigate the effect of the understory reflectance on the retrieval of the canopy LAI. The R^2 between the field-measured LAI and the retrieved LAI is 0.27, under the assumption that the reflectance is uniform for each understory vegetation in the SOBS site. The R^2 increases to 0.78 when the understory reflectance is allowed to vary within the range of variability as determined by field measurements. This result conforms to the sensitivity analysis result in which the at-canopy reflectance is expressed as a function of the understory reflectance at the CASI viewing geometry. The results imply that it is questionable to assume a uniform understory reflectance in canopy model inversions in the boreal forest summer scenes. ©*Elsevier Science Inc., 2000*

INTRODUCTION

The openness of the overstory and spatial and temporal variations of the understory vegetation in boreal forests pose special challenges to the extraction of biophysical parameters of the overstory canopies, such as leaf area index (LAI) and canopy closure, from remotely sensed data. Chen and Cihlar (1996) investigated the correlation between the normalized difference vegetation index (NDVI) derived from TM images and field-measured LAI for the BOREAS (Boreal Ecosystem–Atmosphere Study) flux tower sites. They found that the correlation between NDVI and LAI was small, such as with an R^2 of 0.5 in late spring and 0.42 in mid-summer. Leochel et al. (1997) used helicopter and surface-based radiometric measurements of the boreal forest stands during BOREAS to analyze the relationships of vegetation indices with overstory LAI. Their results show that the correlation between the canopy LAI and vegetation indices is, in general, small with an R^2 of less than 0.3 and confirmed the effects of the understory vegetation on the reflectance of the sparse canopy typical in the boreal forest.

An alternate approach is to retrieve the biophysical parameters characterizing the overstory canopy using a canopy reflectance model. Canopy reflectance model inversion involves adjusting model parameters until the modeled reflectance best fits the measured reflectance (Goel, 1988). A large number of surface reflectance models have been developed in the past decade. They can be divided into four categories: geometric-optical models, radiative-

[*] Department of Physics and Astronomy, York University, Toronto, Canada

† Canadian Space Agency, Saint-Hubert, Quebec, Canada

Address correspondence to Baoxin Hu, Petrie Science Bldg., Room 255, York Univ., 4700 Keele St., Toronto, ON M3J 1P3, Canada. E-mail: baoxin@terra.phys.yorku.ca

Received 22 July 1999; revised 28 February 2000.

REMOTE SENS. ENVIRON. 74:255–274 (2000)

655 Avenue of the Americas, New York, NY 10010

0034-4257/00/$–see front matter
PII S0034-4257(00)00116-4

Table 1. Input and Output Parameters and Intermediate Variables of FLIM

Input parameters	Tree density	n
	Average tree crown radius	R
	Average tree height	H
	Average effective crown leaf area index	L_e
	Geometric factor	$G(\theta_v)$, $G(\theta_s)$
	Solar angles	θ_s, φ_s
	View angles	θ_v, φ_v
	Understory reflectance	$R_g(\lambda)$
	"Homogeneous and infinite" canopy reflectance	$R_c(\lambda)$
Intermediate variables	Crown coverage under θ_v	C_v
	Transmittance under θ_v	T_v
Output	Canopy reflectance	$R(\lambda)$

transfer models, hybrid geometric-optical and radiative-transfer models, and computer simulation models. Most geometric-optical models, such as the Li–Strahler mutual shadow model (Li and Strahler, 1992), and most hybrid geometric-optical and radiative-transfer models, such as the models developed by Li et al. (1995) and by Chen and Leblanc (1997), are developed to describe the reflectance properties of forest canopies. The geometric-optical models greatly simplify the calculation of the at-canopy reflectance by assuming an opaque tree crown, therefore facilitating the inversion process. Studies (Hall et al., 1995; Woodcock et al., 1997) tested the capability of the geometric-optical models in deriving the biophysical parameters of the forest canopies. The hybrid geometrical-optical and radiative-transfer models usually need a large number of physical parameters for the forest canopy, making inversion difficult. Rosema et al. (1992) developed a forest-light interaction model (FLIM) using a first-order approximation of forest canopy reflectance. FLIM accounts for both the effects of shadowing of the overstory and crown transmittance. This model has been applied to TM data of the Kootwijk Forest in the Netherlands to derive LAI and canopy coverage (Rosema et al., 1992). Gemmell and Varjo (1999) investigated the inversion of FLIM using simulated red and near-infrared reflectance data for a wide variety of stand characteristics in the boreal forest. Their results illustrate that the FLIM can be successfully inverted to retrieve the overstory crown coverage and LAI, given understory reflectance and the physical parameters of the

Figure 1. The nomogram of FLIM for the SOBS canopy with the solar zenith angle of 45° and nadir observation. The "homogeneous and infinite" forest canopy reflectance is 0.038 in the red band and 0.23 in the near-infrared band, and the understory reflectance is 0.068 in the red band and 0.17 in the near-infrared band. Points *A* and *B* represent the understory reflectance and "homogeneous and infinite" overstory reflectance in the red and near-infrared band. Each curve shows the variation of the at-canopy reflectance with the increasing of the crown coverage (from top to bottom) at a given crown transmittance.

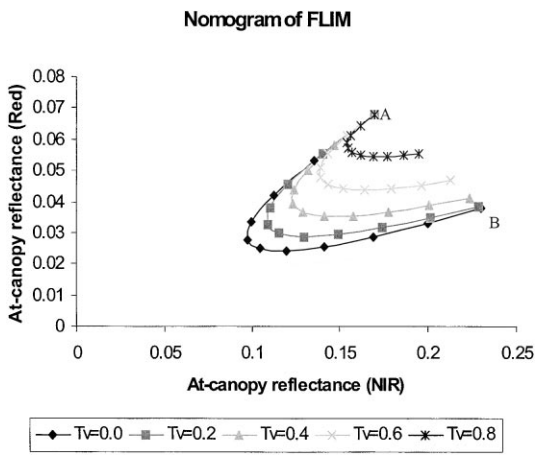

Figure 2. Comparison of the nomogram of FLIM for the SOBS canopy (with an ellipticity of 8.0) between the original version and the modified version. In the legend "Modifying shadow effect" refers to the version where only the effect of the ellipicity of the crown on its shadow on the ground is considered, compared with the original version; and "Modified FLIM" means the final version which takes into account the effects of the ellipicity of the crown on both its shadow on the ground and the transmittance through crowns.

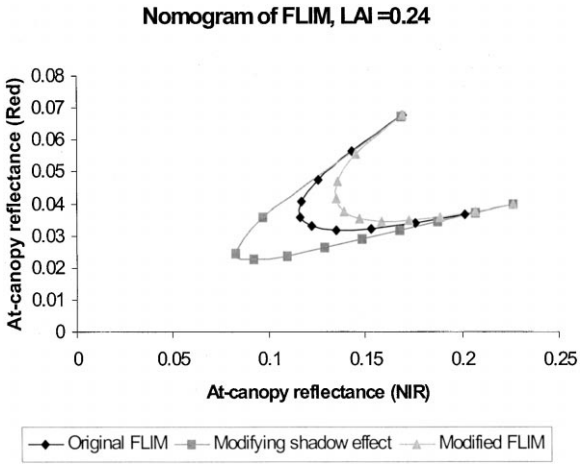

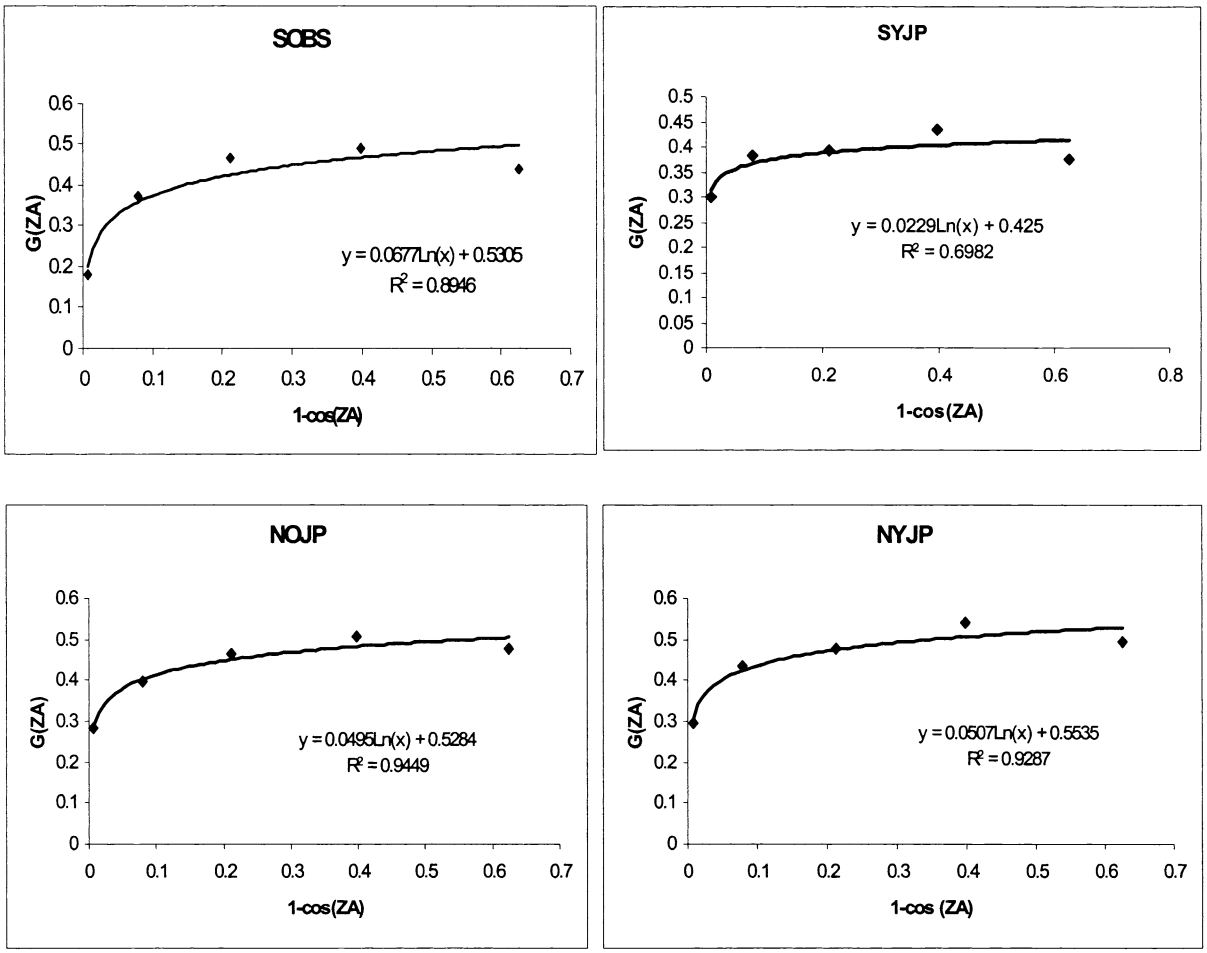

Figure 3. The geometry factor *G*(ZA) (*y*-axis) estimated from the gap fraction measurements and the average LAI values (courtesy J. Chen), where ZA means zenith angle.

tree crown, such as tree height and tree size. The research of Gemmell and Varjo (1999) also shows that the at-canopy reflectance is sensitive to the understory reflectance for TM image viewing geometry and indicates that an important limitation to the success of model inversion may be the variations of the understory reflectance.

This study is to investigate the retrieval of the canopy closure and LAI using FLIM inversion. The high-spatial resolution CASI (Compact Airborne Spectrographic Imager) images over the BOREAS flux tower sites obtained in the winter of 1994 are used, exploiting a relatively uniform and spectrally featureless snow background. The other objective of this study is to investigate the effect of the variations of the understory reflectance on the LAI retrieval using the CASI images obtained in the summer of 1996.

CASI DATA AND STUDY SITES

The CASI airborne pushbroom imaging spectrometer sensor was deployed extensively at BOREAS for acquisition of multispectral imagery in the visible and near-infrared spectral band (Miller et al., 1995). During the BOREAS field campaigns in the winter of 1994 and in the summer of 1996, several CASI images with the spatial resolution of 2 m by 2 m were obtained over flux tower sites in the BOREAS southern study area and northern study area. In this study the CASI images over young jack pine (*Pinus banksiana*) in the southern study area (SYJP), old black spruce (*Picea mariana*) in the southern study area (SOBS), young jack pine in the northern study area (NYJP), and old jack pine in the northern area (NOJP) are employed. These CASI images have been calibrated (Gray et al., 1997), atmospherically corrected (O'Neill et al., 1997), and georeferenced.

The BOREAS southern and northern study regions are located in Saskatchewan and in Manitoba, Canada (BORIS, 1993). The boreal forest and aspen groves dominate the regions. The tower flux sites lie in the areas with relatively homogeneous vegetation cover. In the SYJP site, regenerating Jack Pine with the mean tree height of about 4.65 m comprises the dominant overstory canopy, while the ground is covered with vegetation consisting of bearberry (*Arctostaphylos uva-ursi*), bog cranberry (*Vaccinium vitis-idaea*), and lichen (*Cladina*). The SOBS site is composed of two kinds of stands, black spruce with feather moss

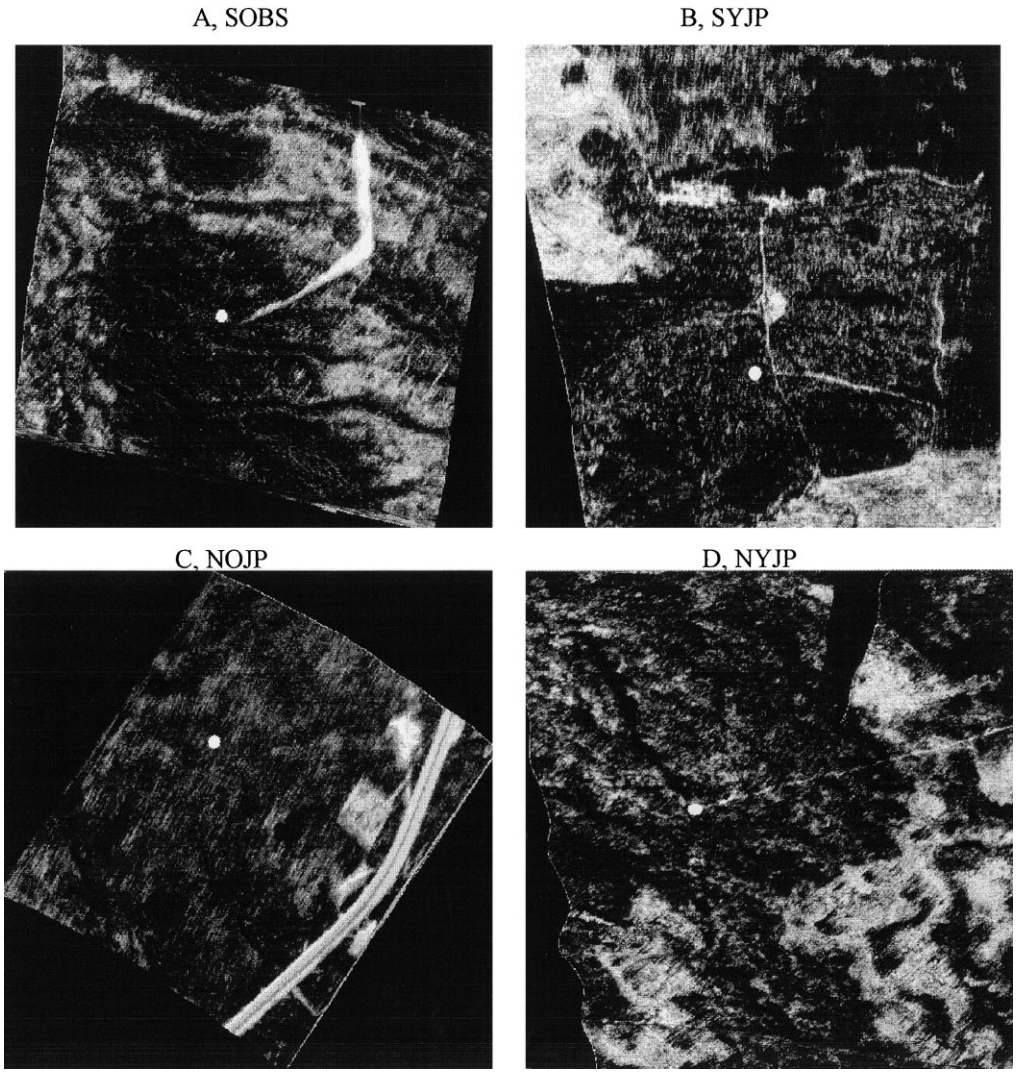

Figure 4. The CASI winter three-band composite images over SOBS, SYJP, NOJP, and NYJP flux tower sites (wavebands centered at 798, 666 and 583 nm). The spatial resolution is 2 m by 2 m for SOBS, SYJP, and NYJP and 1 m by 1 m for NYJP. The tower position for each site is marked.

(*Pleurozium schreben*) understory and black spruce with sphagnum (*Sphagnum fuscum*) understory. In the NYJP site, there are three main cover categories in the Jack Pine stand. The first one is uniform regeneration Jack Pine dominated by young Jack Pine with a height of less than 3 m. The second category has denser Jack Pine coverage than the first. The last one is regenerating vegetation (meadow). The vegetation in the NOJP site is basically Jack Pine forest, ranging from dry, open Jack Pine with lichen on the forest floor, to a more dense Jack Pine with occasional Black Spruce and a forest floor dominated by feather mosses.

FLIM MODEL AND ITS APPLICATION TO THE BOREAL FOREST CANOPY

FLIM Model

FLIM model is a stochastic model developed to describe the bidirectional reflectance properties of forest canopies. It accounts for both the effects of shadowing of the overstory and crown transmittance (Rosema et al., 1992). FLIM expresses the reflectance of the scene viewed by the sensor as the weighted sum of the ground reflectance and the reflectance of a homogeneous and infinitely deep forest canopy (hereafter simply "homogeneous and infinite" canopy reflectance), as shown in the following equation:

$$R = R_c C + R_g G, \quad (1)$$

where R is the reflectance of the scene, R_c and R_g are the "homogeneous and infinite" forest canopy reflectance and understory vegetation reflectance, respectively; and C and G are their corresponding weights called "crown factor" and "ground factor" that are affected by the size of crown, tree density, and leaf area index, and thus are functions of crown coverage and transmittance through crowns.

In FLIM, the crown coverage and crown transmittance in the direction of observation and illumination are calculated by the following equations:

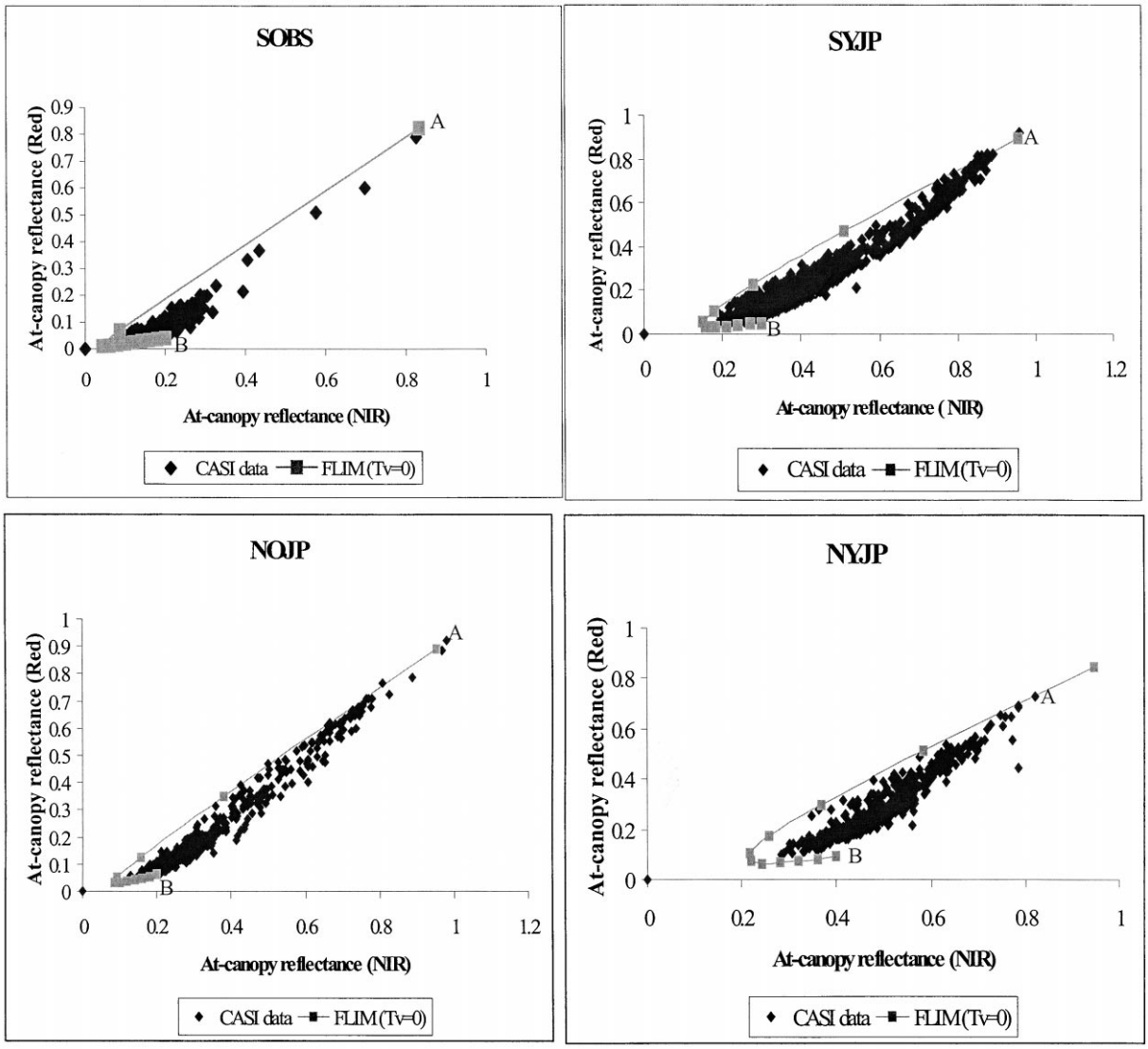

Figure 5. The scatter points of the red reflectance versus near-infrared reflectance and the nomogram of FLIM for the SOBS, SYJP, NOJP, and NYJP sites. Point *A* represents the understory, snow for the sites investigated, and point *B* represents the dense forest stand. The curve *AB* is predicted by FLIM.

$$C_v = 1 - \exp(-nA/\cos(\theta_v)), \quad (2)$$

$$C_s = 1 - \exp(-nA/\cos(\theta_s)), \quad (3)$$

$$T_v = \exp(-G(\theta_v)L_e/\cos(\theta_v)), \quad (4)$$

$$T_s = \exp(-G(\theta_s)L_e/\cos(\theta_s)), \quad (5)$$

where C_v and C_s are the crown coverage in the direction of observation and illumination, T_v and T_s are the transmittance through crowns in the direction of observation and illumination, θ_v and θ_s are the view zenith angle and solar zenith angle, A is the area of the footprint of the sensor's field of view or pixel size, n is the tree density in a pixel; L_e is the average effective leaf area index of crowns and the effective canopy leaf area index is the product of the effective crown leaf area index and the crown coverage at nadir. In the following, the effective leaf area index is also simply called leaf area index. $G(\theta_v)$ and $G(\theta_s)$ are the fraction of total shoot area that is perpendicular to the view zenith angle and the solar zenith angle, respectively. To determine the ground factor, four different ground components are identified: i) the area under crowns in both illumination and observation directions (denoted as F_{cd}), ii) the open space in both illumination and observation directions (F_{os}), iii) the area open in the illumination direction and under crowns in the observation direction (F_{cs}), and iv) the area under crowns in the illumination direction and open to the observation direction (F_{od}). Therefore,

$$G = F_{cd}T_sT_v + F_{cs}T_v + F_{od}T_s + F_{os}. \quad (6)$$

The crown factor is given as follows:

$$C = (1 - T_sT_v)C_sC_v, \quad (7)$$

where F_{ds}, F_{cs}, F_{od}, and F_{os} are functions of C_s, C_v, and a

Table 2. The Parameters Needed To Establish the FLIM Look-Up Tables

	Parameters	*Values*	*Source*
SOBS	Solar zenith angle	75°	Geographic location and the time where and when the data are obtained
	View zenith angle	0°	CASI mission data
	Average radius	0.65 m	Field-measured data
	Average tree height	7.0 m	Field-measured data
	Geometry factor	0.0677 ln (1−cos(θ))+0.531	Field-measured data
	Ellipticity	8.0	Field-measured data
	Understory reflectances in the red and NIR band	0.84, 0.85	CASI images
	The reflectances of the "homogeneous and infinite" overstory canopy in the red and NIR band	0.04, 0.2	CASI images
SYJP	Solar zenith angle	69°	Geographic location and the time where and when the data are obtained
	View zenith angle	0°	CASI mission data
	Average radius	0.85 m	Field-measured data
	Average tree height	4.65 m	Field-measured data
	Geometry factor	0.0229 ln (1−cos(θ))+0.425	Field-measured data
	Ellipticity	2.4	Field-measured data
	Understory reflectances in the red and NIR band	0.9, 0.96	CASI images
	The reflectances of the "homogeneous and infinite" overstory canopy in the red and NIR band	0.05, 0.3	CASI images
NOJP	Solar zenith angle	69°	Geographic location and the time where and when the data are obtained
	View zenith angle	0°	CASI mission data
	Average radius	1.1 m	Field-measured data
	Average tree height	10.5 m	Field-measured data
	Geometry factor	0.0495 ln (1−cos(θ))+0.528	Field-measured data
	Ellipticity	3.0	Field-measured data
	Understory reflectances in the red and NIR band	0.92, 0.97	CASI images
	The reflectances of the "homogeneous and infinite" overstory canopy in the red and NIR band	0.05, 0.2	CASI images
NYJP	Solar zenith angle	75°	Geographic location and the time where and when the data are obtained
	View zenith angle	0°	CASI mission data
	Average radius	0.5 m	Field-measured data
	Average tree height	2.0 m	Field-measured data
	Geometry factor	0.0507 ln (1−cos(θ))+0.554	Field-measured data
	Ellipticity	2.4	Field-measured data
	Understory reflectances in the red and NIR band	0.9, 0.95	CASI images
	The reflectances of the "homogeneous and infinite" overstory canopy in the red and NIR band	0.1, 0.4	CASI images

term describing the hotspot effect. The equations to calculate the four components are given by Rosema et al. (1992).

Equations (1), (6), and (7) constitute the FLIM. Equation (1) has two unknown variables C and G, which can be expressed by C_v and T_v. Table 1 summarizes the input and output parameters and intermediate variables of the forward FLIM. A reflectance nomogram derived from FLIM for the SOBS canopy at a solar zenith angle of 45° and nadir observation is shown in Figure 1. The "homogeneous and infinite" forest canopy reflectance is 0.038 in the red band and 0.23 in the near-infrared band, and the understory reflectance is 0.068 in the red band and 0.17 in the near-infrared band. Points A and B are the locations of the open area and the dense overstory canopy in the plane of red reflectance versus near-infrared reflectance. Each curve shows the variation of the at-canopy reflectance with increasing crown coverage (from top to bottom) at a given crown transmittance (or leaf area index). To invert FLIM for LAI and canopy closure, the at-canopy reflectances at two spectral bands are needed, along with the input parameters in Table 1, except for the tree density n and, of course, L_e.

The Modification of FLIM Model

For the conifer canopies in the BOREAS flux tower sites, tree crowns can be assumed as an ellipsoid with the horizontal radius and vertical radius . The ellipticity (b/r) is large for the crown of these canopies, especially for old Black Spruce. For example, the ellipticity for SOJP, SYJP, and SOBS is about 3.0, 2.4, and 8.0, respectively (Leblanc et al., 1999). As a result, FLIM was modified to account for the effects of crown's shape on the shadows on the ground. Based on the approach used by Li and Strahler (1992), the equations for crown coverage [Eqs. (2) and (3)] were modified in Eqs. (8)–(11) as follows:

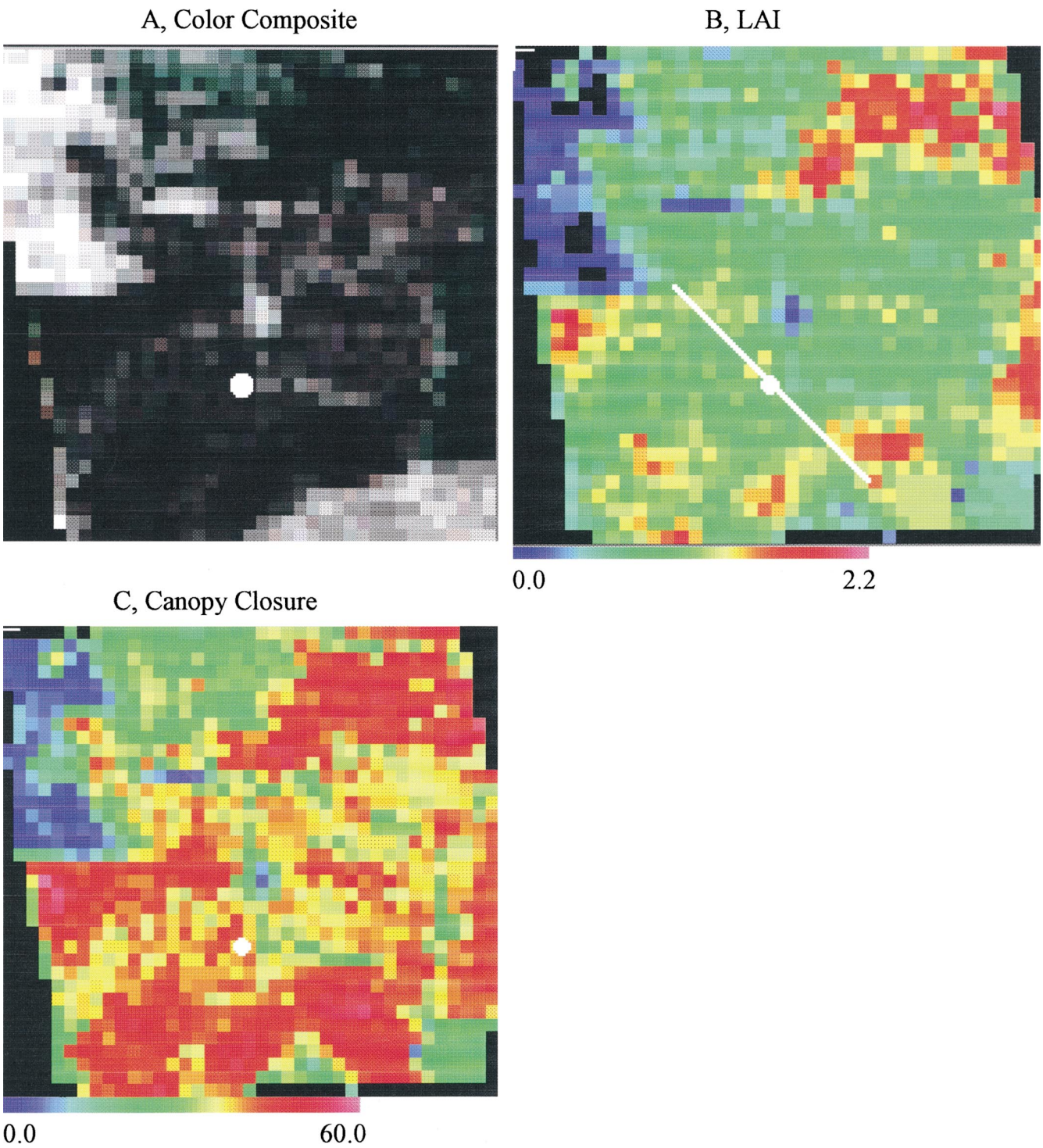

Figure 6. Panel A: the color composite image over the SOBS tower flux site, with the near-infared band (798 nm) printed as red, the red band (666 nm) as green, and the green band (583 nm) as blue. Panel B: the canopy LAI derived from CASI winter image using FLIM. Panel C: the canopy closure derived from CASI winter image using FLIM. The spatial resolution is 30 m by 30 m. The tower position is marked. The transect *B* where Chen et al. (1997) made the LAI measurements is also marked in Panel B.

$$C_v = 1 - \exp(-n\pi r^2/\cos(\theta_v')), \quad (8)$$

$$C_s = 1 - \exp(-n\pi r^2/\cos(\theta_s')), \quad (9)$$

$$\tan(\theta_v') = (b/r)\tan(\theta_v), \quad (10)$$

$$\tan(\theta_s') = (b/r)\tan(\theta_s). \quad (11)$$

The change of the FLIM nomogram between the original version and modified version for the SOBS canopy for a nadir-viewed summer scene with the solar zenith angle of 45° is illustrated in Figure 2. The change made to consider the effect of crown shape on shadows extends the original

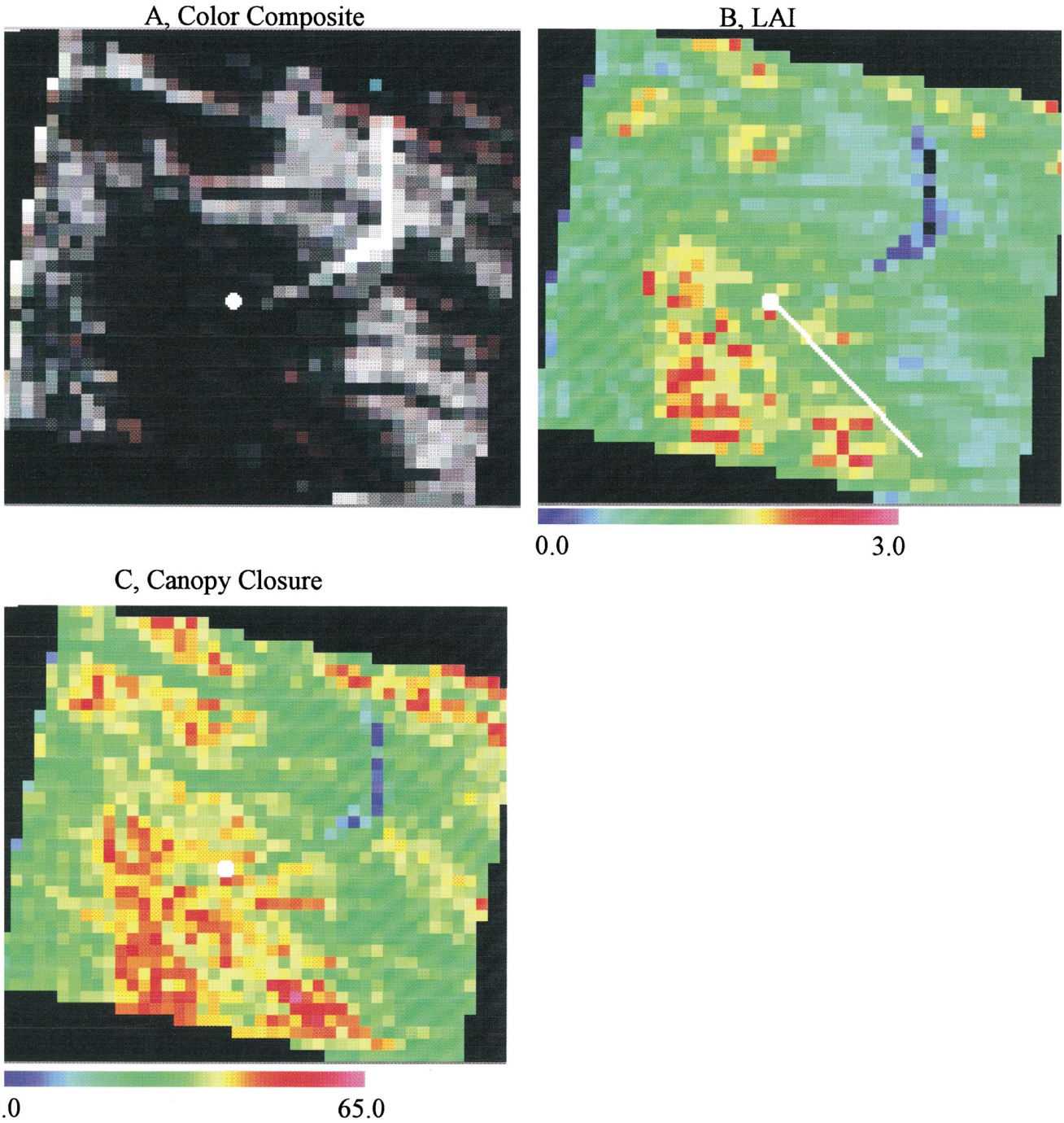

Figure 7. Panel A: the color composite image over the SYJP tower flux site, with the near-infared band (798 nm) printed as red, the red band (666 nm) as green, and the green band (583 nm) as blue. Panel B: the canopy LAI derived from CASI winter image using FLIM. Panel C: the canopy closure derived from CASI winter image using FLIM. The spatial resolution is 30 m by 30 m. The tower position is marked. The transect *B* where Chen et al. (1997) made the LAI measurements is also marked in Panel B.

curve to the origin (dark shadow) direction, which is due to the increasing of the shadows on the ground.

Equations (4) and (5) are valid to calculate the transmittance for horizontally homogeneous vegetation canopy. Following Li and Strahler (1988) and Chen et al. (1997) the effect of crown shape on the transmittance through crowns can be accounted for by means of Eqs. (12) and (13):

$$T_v = \exp\left(-G(\theta_v)L_e\frac{C_{nadir}}{C_v\cos(\theta_v)}\right), \quad (12)$$

$$T_s = \exp\left(-G(\theta_s)L_e\frac{C_{nadir}}{C_s\cos(\theta_s)}\right). \quad (13)$$

In these equations, C_{nadir} is the crown coverage at nadir.

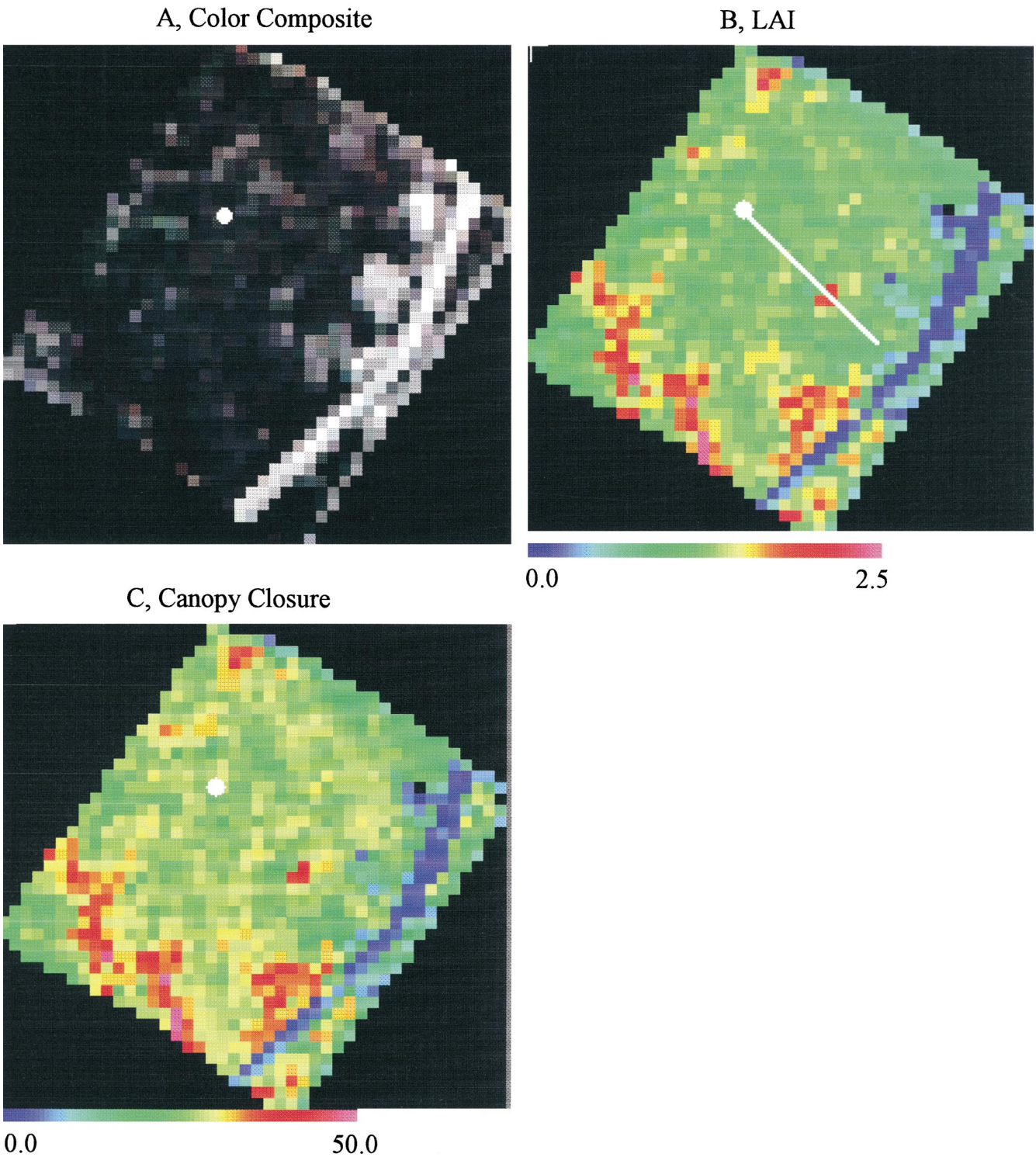

Figure 8. Panel A: the color composite image over the NOJP tower flux site, with the near-infared band (798 nm) printed as red, the red band (666 nm) as green, and the green band (583 nm) as blue. Panel B: the canopy LAI derived from CASI winter image using FLIM. Panel C: the canopy closure derived from CASI winter image using FLIM. The spatial resolution is 30 m by 30 m. The tower position is marked. The transect B where Chen et al. (1997) made the LAI measurements is also marked in Panel B.

The change made to account for the effect of crown shape on the transmittance through the crown decreases the curvature of the curve representing the at-canopy reflectance considering only the effect of the ellipticity of the crown on its shadow on the ground, as shown in Figure 2. This effect arises because the average distance through which the solar radiation passes within the crowns with an ellipsoid shape ($b>r$) is smaller at off-nadir than at nadir views.

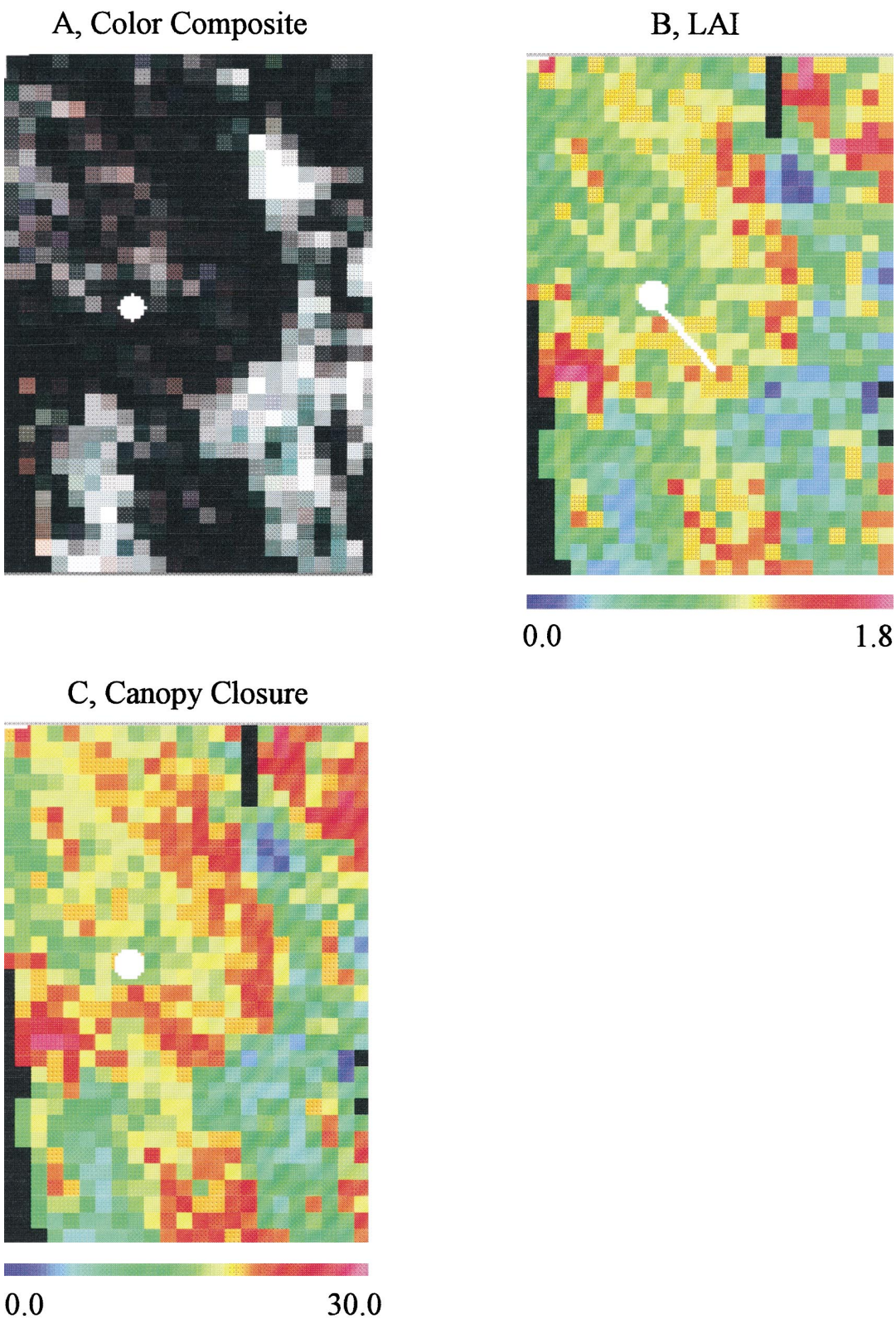

Figure 9. Panel A: the color composite image over the NYJP tower flux site, with the near-infared band (798 nm) printed as red, the red band (666 nm) as green and the green band (583 nm) as blue. Panel B: the canopy LAI derived from CASI winter image using FLIM. Panel C: the canopy closure derived from CASI winter image using FLIM. The spatial resolution is 30m by 30m. The tower position is marked. The transect *B* where Chen et al. (1997) made the LAI measurements is also marked in Panel B.

In these equations, $G(\theta_v)$ and $G(\theta_s)$ account for both the crown shape and the shoot angle distribution.

RETRIEVAL OF LAI AND CANOPY CLOSURE FROM CASI WINTER IMAGES USING FLIM

Estimation of the Geometry Factor

In this study, the foliage angle distributions for the canopies investigated (SYJP, SOBS, NYJP, and NOJP) were estimated based on gap fraction measurements with the Li-Cor LAI-2000 instrument.

LAI-2000 measures canopy gap fraction based on diffuse blue light transmission through the canopy at five zenith angles (7°, 23°, 38°, 53°, and 67°). Theoretically, the gap fraction $p(\theta)$ at the zenith angle of θ is as follows, assuming that shoots for conifers are arranged spatially in a random distribution:

$$p(\theta)=e^{-G(\theta)L_e/\cos\theta}. \tag{14}$$

From Eq. (14), it is clear that, in the absence of the knowledge of the shoots angle distribution, LAI can be calculated by the following equation if the gap fraction is measured at several zenith angles:

$$L_e=\int_0^{\pi/2}\ln\left(\frac{1}{p(\theta)}\right)\cos\theta\,\sin\theta\,d\theta. \tag{15}$$

For the LAI-2000, the gap fraction is measured at five zenith angles, and thus the geometry factor can be estimated via Eqs. (14) and (15). The gap fraction was measured with the LAI-2000 along three transects during the BOREAS 93 campaign (IFC-3) (J. Chen, personal communication). Based on the gap fractions at the five angles and the average effective LAI (courtesy J. Chen), the geometry factors for the canopies investigated were calculated and are shown in Figure 3. The shape of is mainly determined by the vertical shoot angle distribution for the SYJP, NYJP, and NOJP canopies (Chen, 1996), while it is mainly determined by the crown shape for the SOBS canopy.

From Figure 3, one can note that the average $G(\theta)$ is less than 0.5 for all of the sites investigated. Whereas it is true that $G(\theta)$ is averaged to about 0.5 for planar leaves (Asrar, 1989), this statement may be not correct for conifers. Nilson and Ross (1997) discussed the relative geometric cross section (RGCS) for needles and shoots for conifer canopies. The RGCS is considered equivalent to the G-function for the planar leaves. Their results showed that for a spherical needle axis distribution, RGCS is 0.5, while RGCS of spherically distributed shoots for Scots pine was found to be approximately 0.32. The average shoot RGCS was shown to be less than 0.4 for different shoot angles, such as for horizontal shoots or vertical shoots. Our results appear to be consistent with this recent theoretical work.

Retrieval of LAI and Canopy Closure from FLIM

CASI images used for this study were obtained in the winter of 1994 over SYJP, SOBS, NYJP, and NOJP sites at large solar zenith angles (>70°), due to the high latitude of these sites. For application of a canopy BRDF model, such as FLIM, the original 2 m by 2 m CASI images were spatially degraded to a spatial resolution of 30 m by 30 m, in order to ensure that a tree crown and its shadow occur in the same pixel, with the very large solar zenith angles characteristic of this winter imagery. The high spatial resolution CASI images are shown in Figure 4 and their degraded images are shown in the left-upper panels of Figures 6, 7, 8, and 9.

As previously noted, at least two spectral bands are needed to invert FLIM. In this study, the near-infrared band (798 nm) and the red band (666 nm) are used, and the scatter plot of red reflectance versus the near-infrared reflectance for SOBS, SYJP, NOJP, and NYJP are shown in Figure 5. Point *A* in these plots represents the understory, snow for the sites investigated, since the reflectance of snow is high in both the red band and the near-infrared band. Point *B* represents the dense forest stand that has higher reflectance in the near-infrared band than in the red band. Based on the scatter plots and the CASI images shown in Figure 4, the "homogeneous and infinite" canopy reflectance and the understory reflectance (snow reflectance), "end points," are estimated. The physical parameters of the crown, such as the average radius, average tree height, and ellipticity, are estimated based on the information provided in the BOREAS home page (http:/boreas.gsfc.nasa.gov) and from Leblanc et al. (1999). Given these parameters, a look-up table is established for each site with the intermediate variables in FLIM (Table 1) as input and the at-canopy reflectance in the red and near-infrared band as output. Thus, for a series of C_{nadir} (for the cases investigated, C_{nadir} and C_v are equal) and T_v values, the corresponding at-canopy reflectance in the red and near-infrared bands can be calculated. Table 2 provides the parameters for these sites investigated. The curve *AB* in Figure 5 is predicted by FLIM for the SOBS, SYJP, NOJP, and NYJP sites, with a very little transmittance (T_v). Each scatter point represents the pixel with a variable crown coverage and a variable crown transmittance, and these values can be calculated based on the look-up-table established.

It is worth mentioning that the determination of the "end points," R_c and R_g, is difficult based just on the 30 m resolution images without knowledge of the crown coverage of the site investigated. Rosema et al. (1992) and Gemmel and Varjo (1999) estimated the "end points" based on known forest characteristics for some plots in the site of interest. In this study, 2 m high spatial resolution CASI images were examined to locate regions of the dense canopy and to estimate its crown coverage at a 30 m spatial resolution, and thereby to estimate values for reflectance of the "homogeneous and infinite" canopy reflectance. The estimated values are adjusted to fit the scatter points shown in Figure 5. An alternate method is based on a radiative transfer model. For example, the "homogeneous and infi-

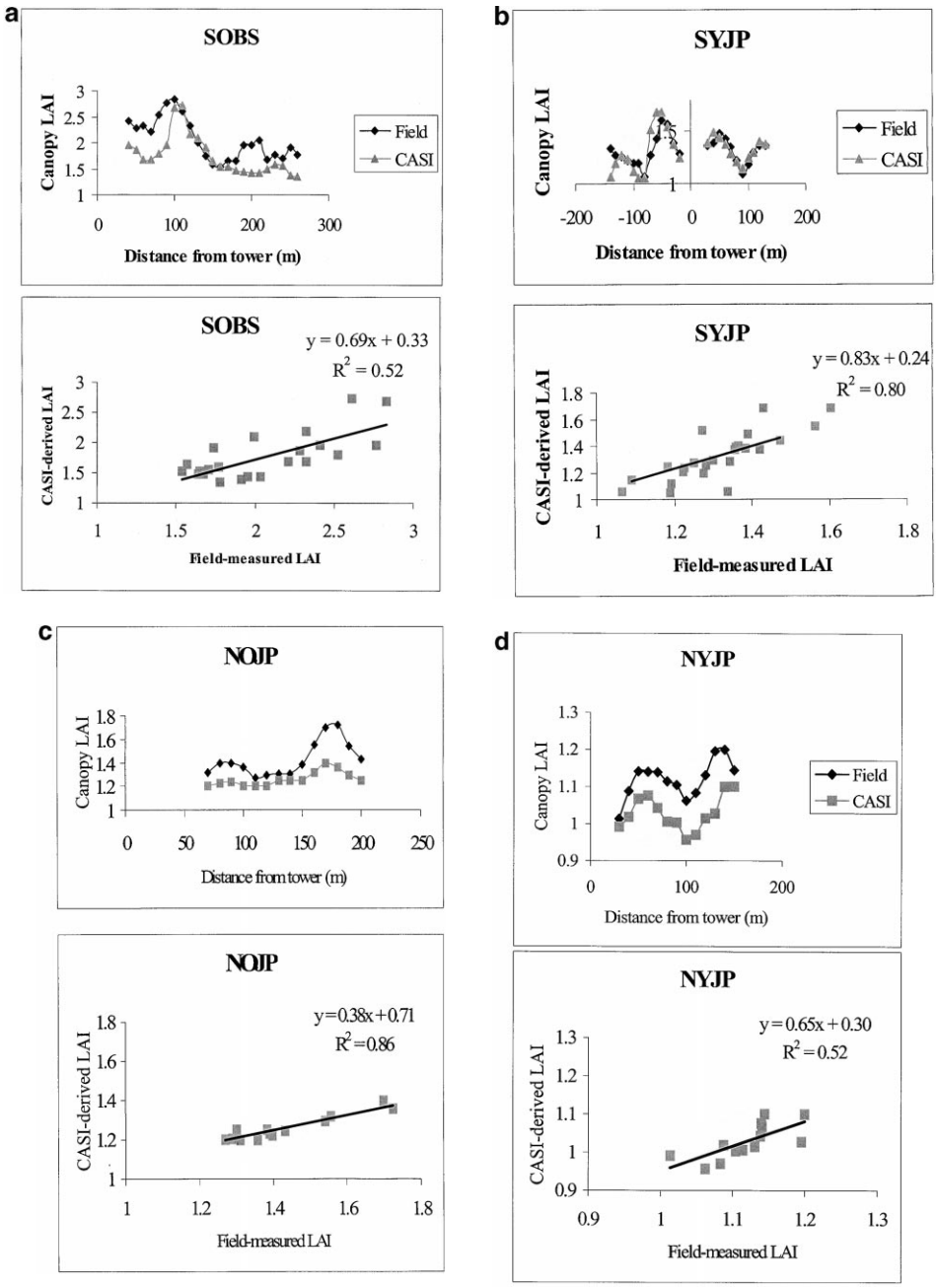

Figure 10. (a) The canopy LAI derived from CASI winter image over the SOBS site and its correlation with the field-measured LAI (Chen et al., 1997); (b) The canopy LAI derived from CASI winter image over the SYJP site and its correlation with the field-measured LAI (Chen et al., 1997); (c) The canopy LAI derived from CASI winter image over the NOJP site and its correlation with the field-measured LAI (Chen et al., 1997); (d) The canopy LAI derived from CASI winter image over the NYJP site and its correlation with the field-measured LAI (Chen et al., 1997).

nite" canopy reflectance can be obtained from the SAIL model (Verhoef, 1984), if the properties of needles, such as reflectance, transmittance, and leaf angle distribution are known. Although the snow reflectance is relatively uniform, it still varies with some factors, such as snow age and snow depth. Furthermore, the apparent sunlit snow reflectance (i.e., as seen from above the canopy) is a function of canopy closure and height (Soffer et al., 1995). From Figure 5, one can note that few sunlit snow pixels are presented in the 30 m spatial resolution images. To obtain the typical snow reflectance for each site, the 2 m spatial resolution images were used to locate enough sunlit snow pixels to calculate the mean value of the reflectance of these pixels. Further research is needed to integrate the magnitude of the variations of the understory reflectance and the "homogeneous and infinite" canopy reflectance in

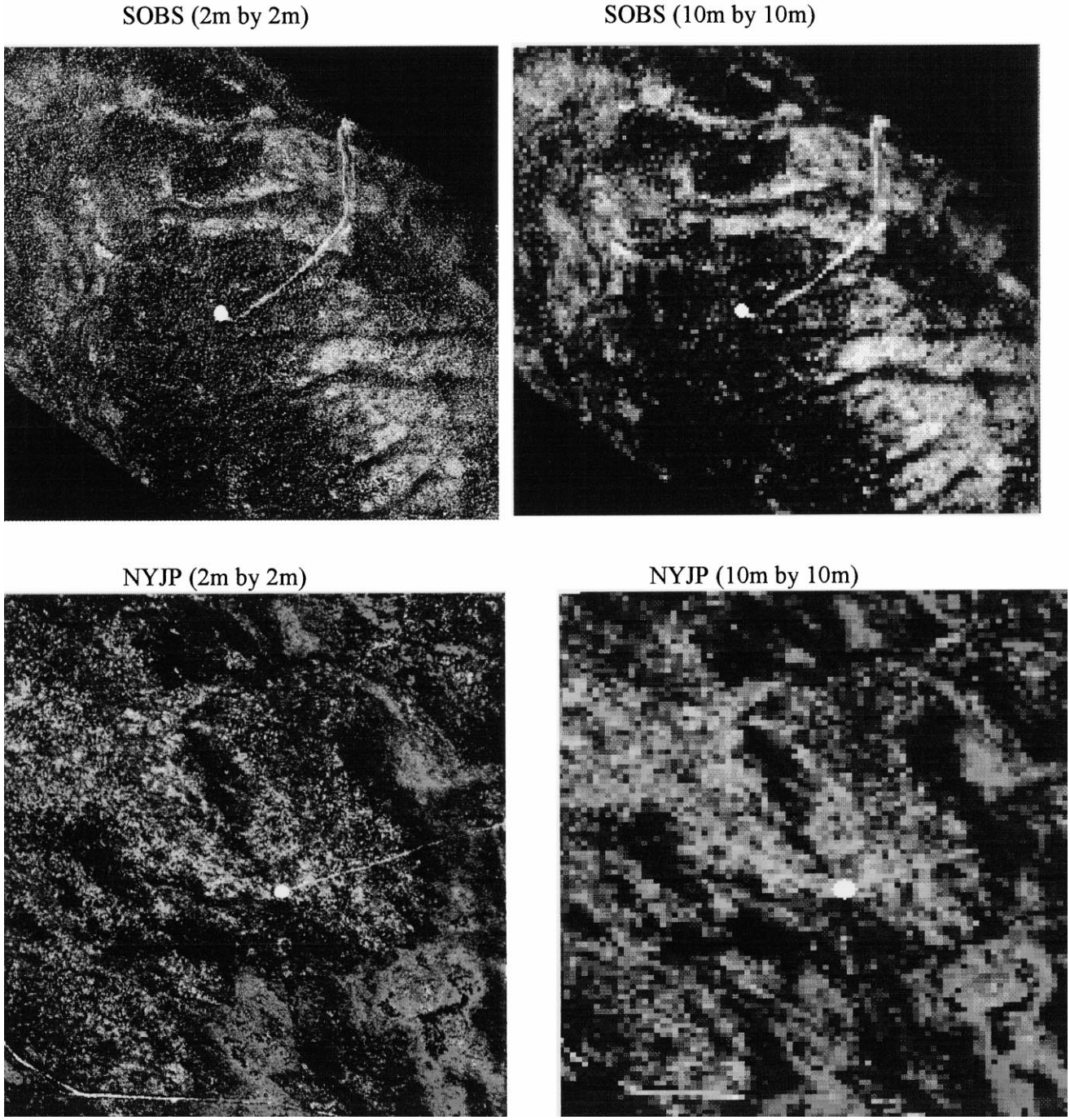

Figure 11. The three-band composite images over the SOBS and NYJP flux tower sites (wavebands centered at 747, 645, and 530 nm). The tower position is marked.

the model or in the model inversion process, in order to improve the quality in the canopy model inversion considering their effects on the model inversion (Gemmel and Varjo, 1999).

Canopy LAI

In this study, the view zenith angle is assumed to be constant at 0°, and thus Eq. (12) can be simplified to Eq. (16):

$$T_v = \exp\left(-\frac{G(\theta_v)L_e}{\cos(\theta_v)}\right). \quad (16)$$

Since L_e is the average crown LAI, the canopy LAI is $C_{nadir}L_e$. The upper-right panels of Figures 6, 7, 8, and 9 show the canopy LAI derived for the four tower-sites. Evident spatial patterns can be observed from these panels, which are similar to those observed in the upper-left panels (color composite images). Basically, the white pixels in the color composite images have lower canopy LAI values, compared with other pixels.

The derived canopy LAI was also quantitatively evaluated using the field-measured canopy LAI with the LAI-

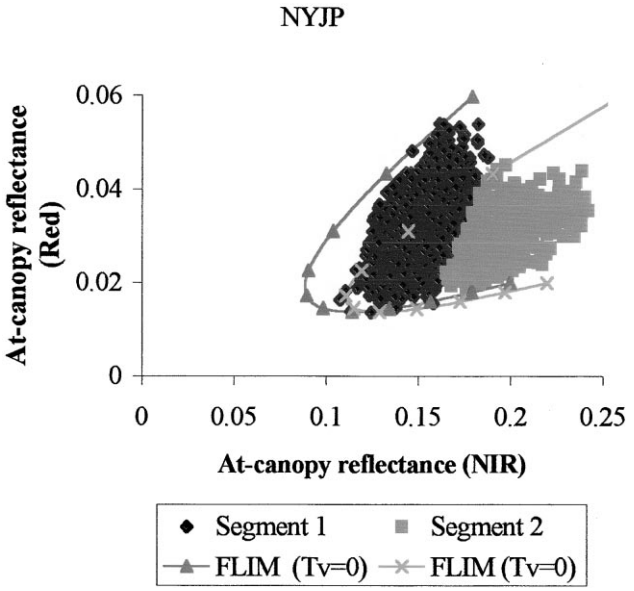

Figure 12. The scatter points of the red reflectance versus near-infrared reflectance from the CASI summer image with the spatial resolution of 10 m by 10 m and the nomogram of FLIM for the NYJP site. Note that there are two classes for the NYJP sites.

2000 by Chen et al. (1997). The canopy LAI values at the four tower sites were measured every 10 m along transects *A*, *B*, and *C* during the BOREAS IFC in 1993. The location of transect *B* is marked in Panel B of Figures 6, 7, 8, and 9, and transects *A* and *C* are parallel to transect *B* with a separation distance of 10 m to each side [see Chen et al. (1997) for details]. For comparison of the field-measured LAI values and the retrieved LAI values (with a spatial resolution of 30 m by 30 m), the field-measured LAI values were averaged. First the field-measured LAI values along each transect were subjected to a sliding average of three measurements (separated by 20 m), and then the resulting values were averaged between the three parallel transects. Figure 10 provides the comparison results between the canopy LAI derived from CASI data using FLIM and the field-measured LAI. The upper panels show that the derived LAI, in general, reproduces the spatial patterns observed in the field-measured LAI. From the lower panels one can note that the derived LAI values shows good consistency with the field-measured LAI values with R^2 of 0.52 for SOBS, 0.80 for SYJP, 0.86 for NOJP, and 0.52 for NYJP.

Although these correlations demonstrate the efficacy of the inverse physical modeling approach to retrieve LAI using suitable multispectral imagery, it is instructive to examine these correlations more closely. For example, it is clear that some bias exists between the field-measured LAI and the derived LAI. First, the intercepts of the regression fit depart from zero and are 0.33, 0.24, 0.71, and 0.30 for SOBS, SYJP, NOJP, and NYJP, respectively. The positive bias is small in all cases, except for NOJP, but is systematic. Second, the slope between the variations in derived LAI relative to field-measured LAI shows appreciable departures from unity with slopes of 0.69, 0.83, 0.38, and 0.65 for SOBS, SYJP, NOJP, and NYJP, respectively. Part of the latter departure from expected behavior might be attributed to the small range in LAI values in the canopies under study. So if the relationship between derived and field LAI values is constrained to go through zero and the regressions recalculated, values of slopes increased to 0.85, 1.01, 0.74, 0.92 while the R^2 decreased to 0.49, 0.76, 0.74, and 0.43 for SOBS, SYJP, NOJP, and NYJP, respectively. This recalculation suggests that the initial NOJP results are probably adversely affected by the limited range in LAI values rather than representing a particularly anomalous retrieval result.

The biases that do remain between retrieved and field LAI values may be caused by the approximations of FLIM and the adjacency effect according to following considerations: 1) FLIM does not consider multiple scattering between leaves and between tree crowns and the understory. The latter may be quite large for the cases investigated, because of the large reflectance of snow. 2) The mutual shadowing between the tree crowns is not considered in FLIM. 3) Although the snow reflectance is relatively uniform, compared with other understory vegetation, the variations in the snow reflectance across the sites may still have effects on the retrieval of the canopy LAI. 4) The adjacency effect caused by the atmospheric scattering and the large contrast between the canopy reflectance and the snow reflectance is not removed in the preprocessing of the CASI winter images. In future studies, these aspects need to be considered to improve the retrieval of the canopy LAI. Other potential reasons for the bias between the retrieved LAI and field-measured LAI may the difference in the scale or spatial resolution between them, and the errors in the georegistration of the CASI images.

Canopy Closure

In FLIM, C_{nadir} is referred to as the crown coverage without considering the within-crown gap probability. For the canopies with clustered needles and small crown LAI, the within-crown gap probability is an important contributor to the crown reflectance properties. In this study, the canopy closure was calculated to take into account both within-crown and between-crown gap probability. Accordingly, the canopy closure can be represented by $C_{\text{nadir}}(1-T_v)$. The lower-left panels in Figures 6, 7, 8, and 9 show the canopy closure for the four tower sites. As these panels show, the canopy closure images are consistent with the observations obtained from the color composite images and the canopy LAI images.

INVESTIGATION OF THE EFFECT OF THE VARIATIONS OF THE UNDERSTORY REFLECTANCE ON THE RETRIEVAL OF THE OVERSTORY CANOPY LAI

Retrieval of the Canopy LAI and Canopy Closure from CASI Summer Images Using FLIM

The CASI 2 m by 2 m summer images over the SOBS and NYJP sites were spatially degraded into images with a spatial resolution of 10 m by 10 m to be used to derive

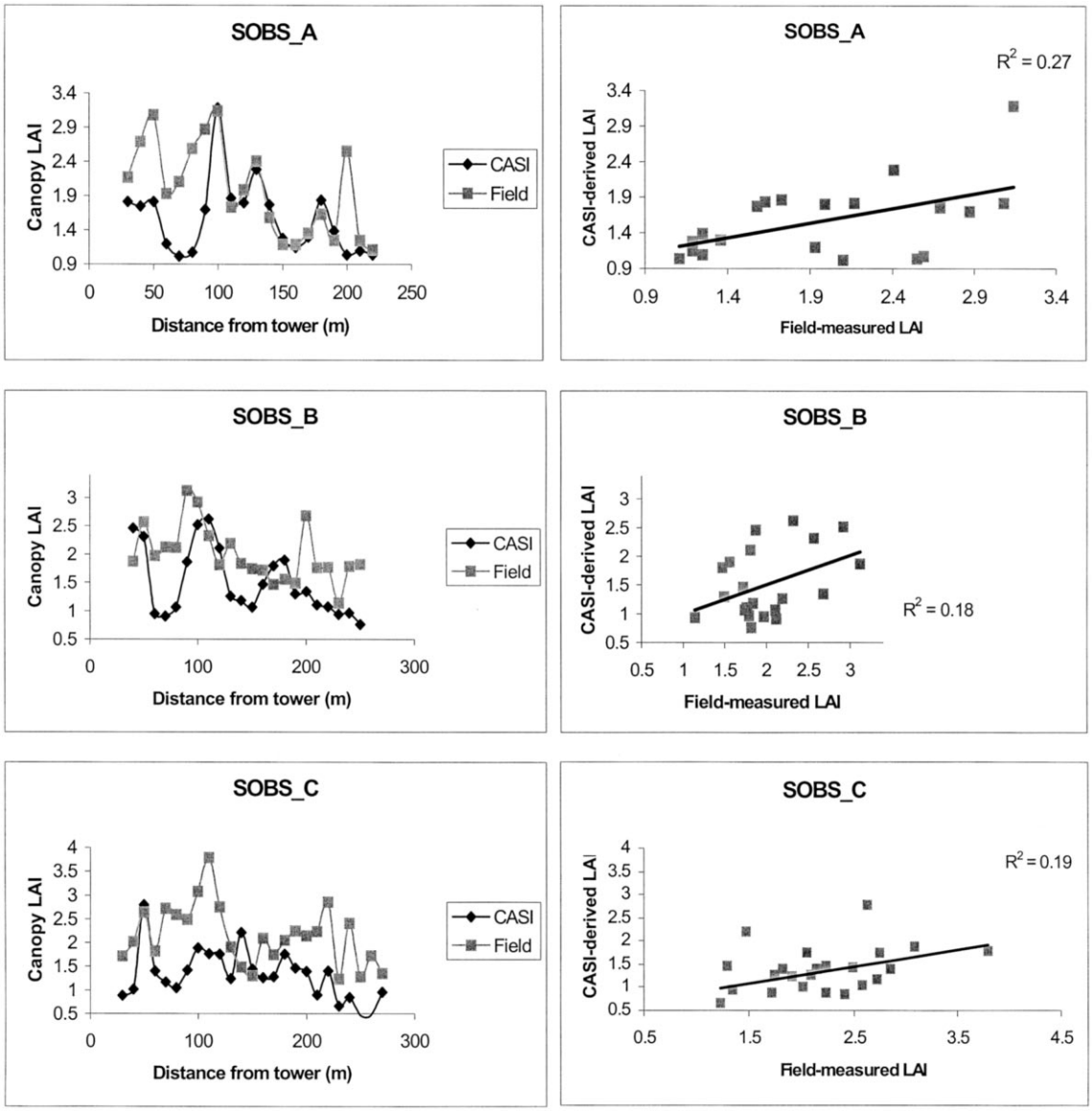

Figure 13. The canopy LAI derived from CASI summer image over the SOBS site using FLIM and its correlation with the field-measured LAI (Chen et al., 1997). The understory reflectance is assumed to be uniform for each understory vegetation.

the canopy LAI and canopy closure using FLIM. With the much higher sun elevation angles in the summer (typically >60°), as compared to the winter data (<20°), the criteria for canopy model retrievals that pixels be of a size to contain both sunlit crowns and the shadows cast on the ground was considered met with a 10 m pixel. The color composite images of the high spatial resolution CASI images are displayed in Figure 11 along with their degraded images. FLIM assumes a uniform understory reflectance across the site of interest. However, there are two classes of understory vegetation in the SOBS site (feather moss at the relatively dense stands and sphagnum at the relatively sparse stands) and in the NYJP site (moss at the relatively dense stands and lichen at the relatively sparse stands). The images shown in Figure 11 clearly exhibit the two strata of stands with different overstory coverage and understory vegetation. The summer images for the entire SOBS and NYJP sites, therefore, are segmented into two classes and require application of FLIM separately for the two classes. The scatter plot of the near-infrared reflectance and the red reflectance from the CASI image over the NYJP site and the nomogram of FLIM are shown in Figure 12 as an example.

Based on the same approach as that employed to invert FLIM from CASI winter images, the canopy LAI and canopy closure over the SOBS and NYJP sites were retrieved from the CASI summer images. The "homogeneous and infinite" overstory reflectance and the understory reflectance are determined using CASI 2 m images and the spatially degraded images, as described above. The understory reflectance for the SOBS site is 0.068 in the red

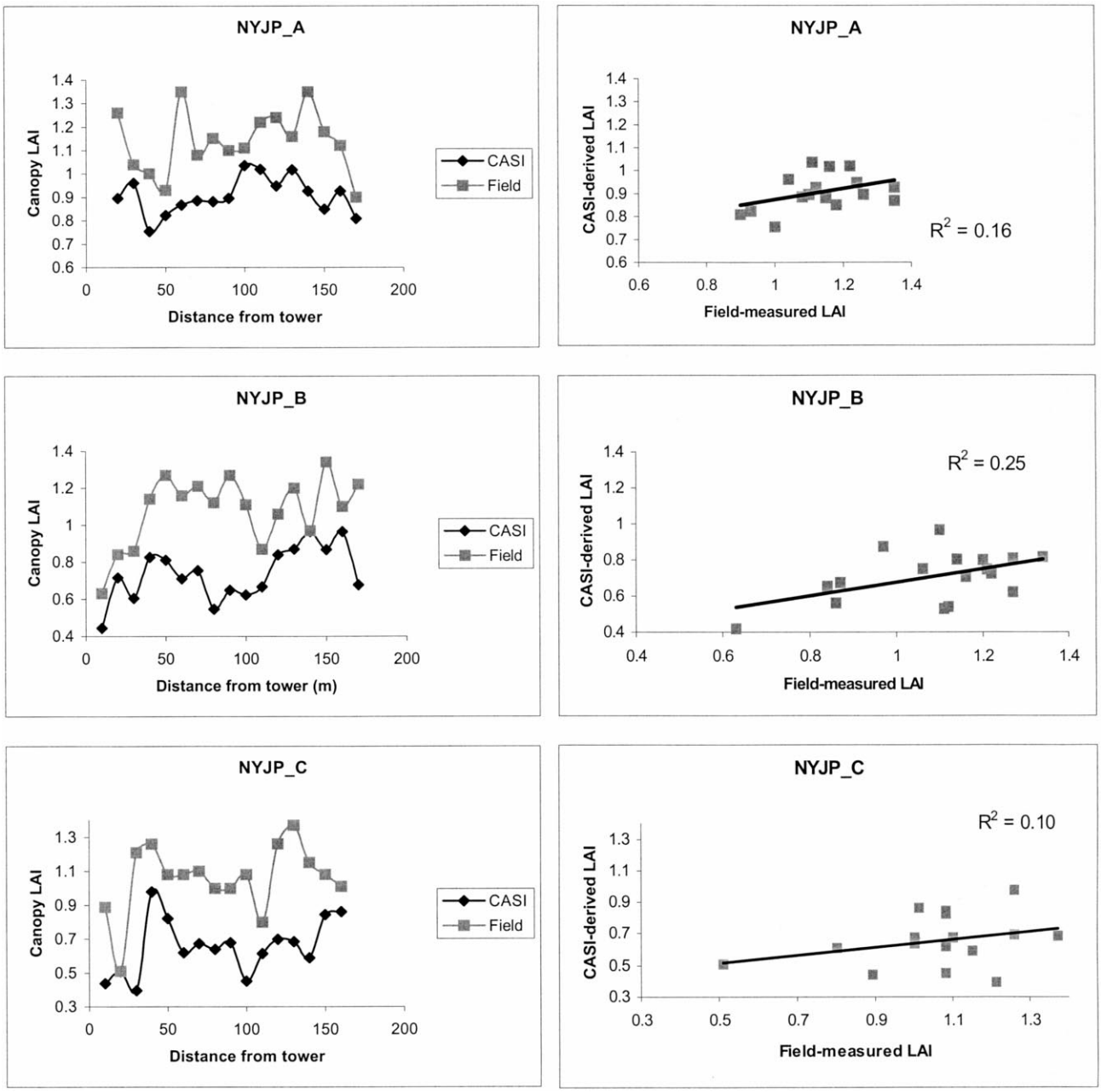

Figure 14. The canopy LAI derived from CASI summer image over the NYJP site using FLIM and its correlation with the field-measured LAI (Chen et al., 1997). The understory reflectance is assumed to be uniform for each understory vegetation.

band and 0.17 for the NIR band for the first segment and 0.12 in the red band and 0.38 in the NIR band for the second segment. The understory reflectance for the NYJP site is 0.06 in the red band and 0.18 for the NIR band for the first segment and 0.06 in the red band and 0.26 in the NIR band for the second segment. The derived LAI was compared with that obtained by Chen et al. (1997) for transects *A*, *B*, and *C*. The results, shown in Figures 13 and 14, indicate that the LAI derived from CASI summer images show overall poor consistency with the field-measured LAI, with the R^2 less than 0.27 for both SOBS and NYJP sites, compared to values greater than 0.5 for the same winter sites.

The retrieved canopy LAI image for the SOBS site was also compared with that produced by Chen et al. (1999) using a CASI 2 m by 2 m image obtained in May 1994. Chen et al. (1999) derived an empirical equation between the canopy LAI and the simple ratio calculated from the CASI image. The equation was developed based on the field-measured canopy LAI values along transects *A*, *B*, and *D*, and the average understory reflectance along transect *B* (Miller et al., 1997). The R^2 between the simple ratio and

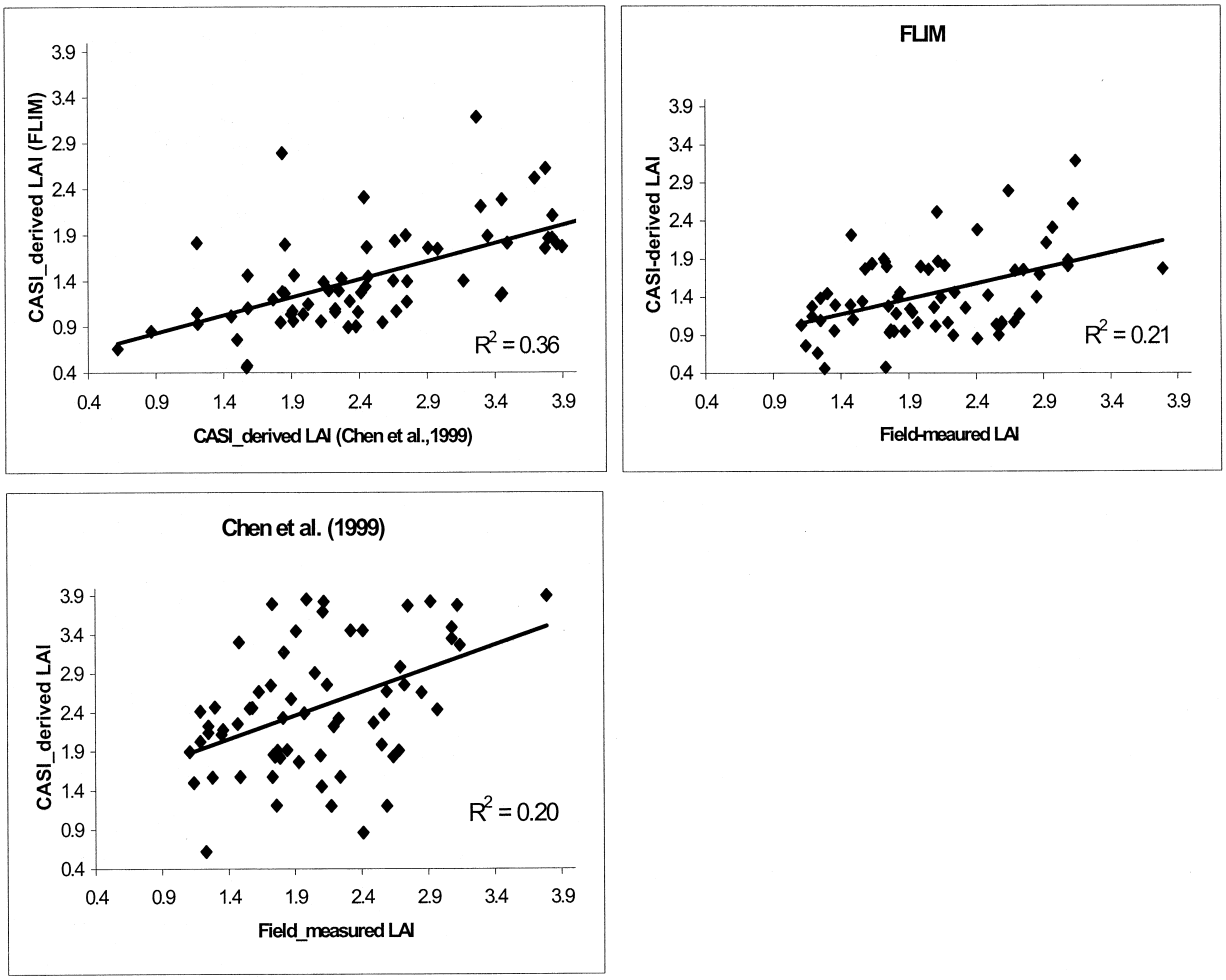

Figure 15. The correlation between the retrieved canopy LAI using FLIM and that from Chen et al. (1999), and the correlation between each of them and the field-measured canopy LAI.

the canopy LAI is 0.26 for transects *A*, *B*, and *D* (Chen et al., 1999). The correlation between the retrieved canopy LAI by FLIM and that calculated by Chen et al. (1999) for the transects *A*, *B*, and *C* is illustrated in Figure 15. The correlation between them is weak with the R^2 of 0.36, as is the correlation between each of them and the field-measured canopy LAI. This could be the result of the effects of variations of the understory reflectance within each class, such as feather moss and sphagnum for SOBS, in the summer images. Miller et al. (1997) measured the average sunlit understory reflectance along transect *B* in the two sites during the summer of 1994. Their results indeed show considerable variability in average understory reflectance with a standard deviation of 0.035 in the red band and 0.065 in the near-infrared band for the SOBS site and 0.047 in the red band and 0.055 in the near-infrared band for NYJP.

Investigation of the Effect of the Understory Reflectance on the Retrieval of the LAI

The sensitivity of the at-canopy reflectance to the understory reflectance in the red and near-infrared bands and to the canopy LAI was analyzed using FLIM for the SOBS canopy, given the defining physical parameters (Table 2), for a range of crown coverage from 0.1 to 0.9. The nominal understory reflectance in the red and near-infrared bands are 0.068 and 0.17. The results shown in Figure 16 indicate that the at-canopy reflectance is sensitive to the observed variability in the understory reflectance. In order to investigate the effect of the understory reflectance on the LAI retrieval, we allow the understory reflectance to vary along the transects and calculate LAI values based on the assumed understory reflectance. Since only the mean and standard deviation of the understory reflectance along the transect *B* are available for this study, for each point along the transect the understory reflectance is allowed to change from 0.048 to 0.088 in the red band and from 0.15 to 0.19 for the NIR band (Miller et al., 1997) to permit the retrieved LAI to approach the field-measured LAI. The comparison between this "adjusted" derived-LAI and the field-measured LAI is shown in Figure 17. It is clear that the derived LAI with a varying understory reflectance is consistent with the field-measured LAI, and characterized by the R^2 larger than 0.64.

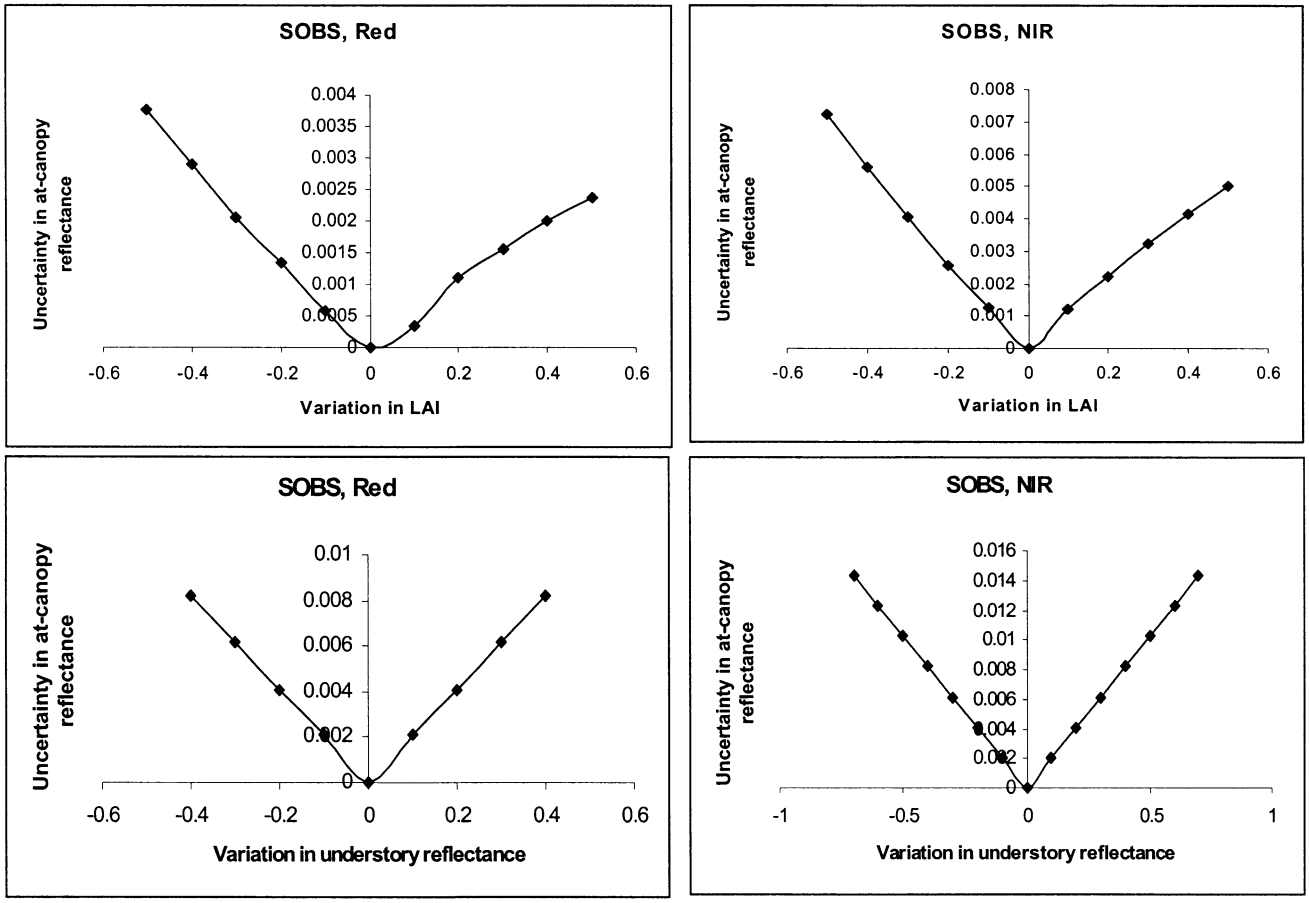

Figure 16. The uncertainty in the at-canopy reflectance caused by the variation in LAI (upper panels) and by the variation in the understory reflectance (lower panels) for the SOBS canopy. The ranges of the variations of the LAI and understory reflectance are from the field measurements (Chen et al., 1997; Miller et al., 1997).

CONCLUSIONS

In this study, retrievals of the canopy LAI and canopy closure from the CASI images using a canopy model were investigated. The original FLIM was adapted to describe the surface reflectance properties of the canopies investigated by considering the effect of the large ellipticity of the conifer crowns on the shadows and crown transmittance. Furthermore, a sensitivity analysis indicates that the at-canopy reflectance is more sensitive to the understory reflectance than to the canopy LAI at the CASI viewing geometry (nadir observation). This result challenges the viability of LAI retrievals using the canopy reflectance model from the summer images where the understory reflectance exhibits evident variations as in the boreal forest sites investigated. The CASI summer image over the SOBS site was used to investigate the effect of the understory reflectance on the retrieval of the canopy LAI. The correlation coefficient between the field-measured LAI and the retrieved LAI under the assumption of a uniform reflectance for each understory vegetation (feather moss or sphagnum) is as low as 0.27. The correlation coefficient increases to 0.78 when the understory reflectance is allowed to vary within the range of the mean value plus or minus its standard deviation obtained by field measurement (Miller et al., 1997).

The CASI winter images were employed to retrieve the LAI and canopy closure, exploiting the relatively uniform snow background. A visual evaluation indicates that the canopy LAI and canopy closure reflect the spatial distribution of the different strata of the forest stands at the sites investigated. The between the retrieved canopy LAI and the field-measured LAI along the transect (Chen et al., 1997) is 0.52 for SOBS, 0.64 for SYJP, 0.86 for NOJP, and 0.51 for NYJP.

The latter results show that the high-spatial resolution CASI winter data provide a good opportunity to map the canopy LAI and canopy closure using a canopy BRDF model inversion approach. The low sun elevations, however, imply that such retrievals are only possible at a degraded spatial resolution, with 30 m spatial resolution demonstrated in this case.

In a future study, the CASI winter images and summer

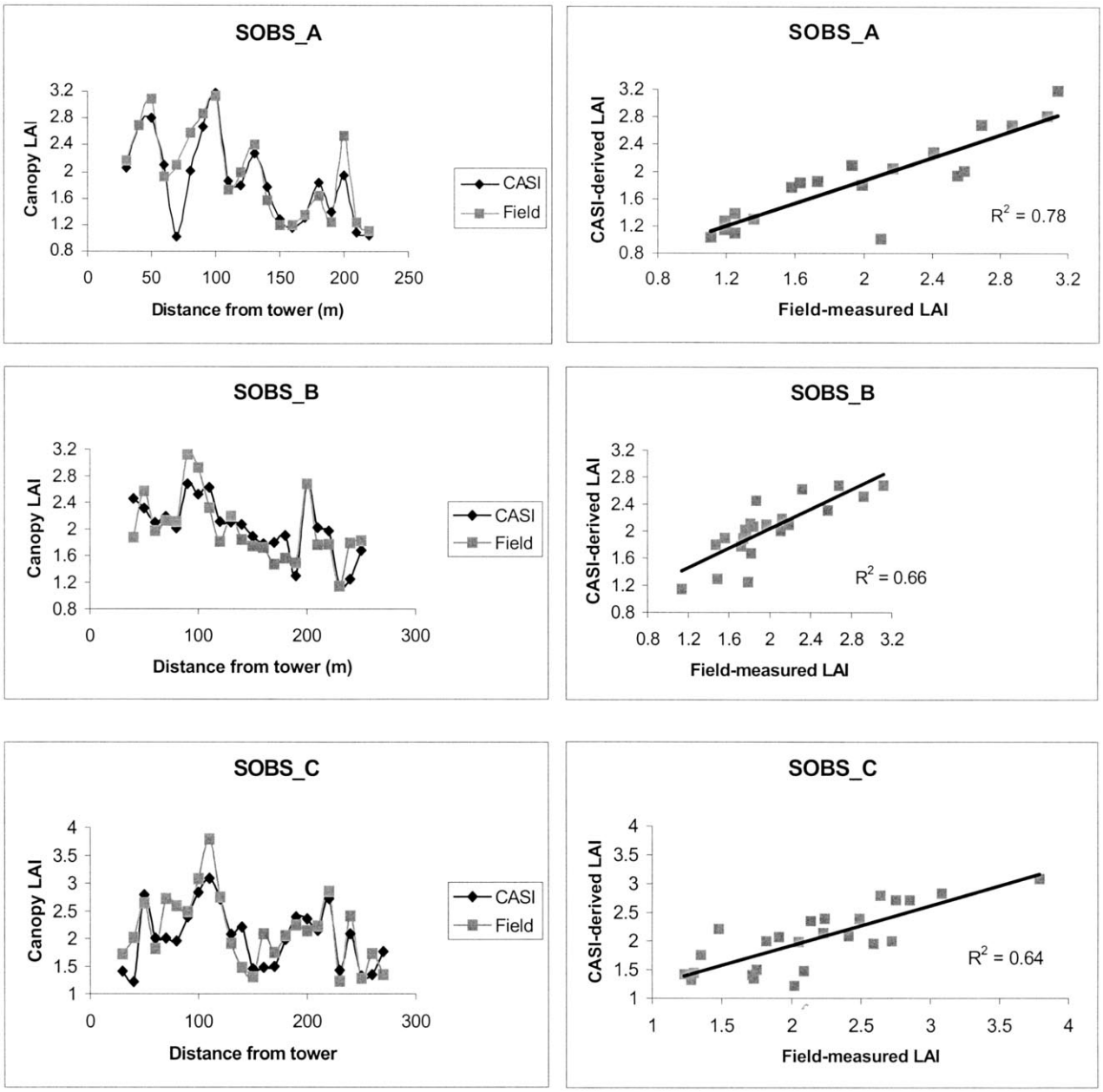

Figure 17. The canopy LAI derived from the CASI summer image over the SOBS site from FLIM. The understory reflectance along the transects varies within the range of the mean value plus or minus its standard deviation obtained by Miller et al. (1997).

images will be integrated to attempt to map the spatial variation of the understory vegetation categories at these boreal forest sites.

We are indebted to Dr. Jing Chen of Canada Centre for Remote Sensing for the LAI-2000 data-gap fraction, and average LAI data. We gratefully acknowledge the Canadian Space Agency for support to participate in the BOREAS Follow-On Program. The CASI processed data available for this study are due to extraordinary efforts of scientists at the Centre for Research in Earth & Space Technology, Jim Freemantle and Lawrence Gray.

REFERENCES

Asrar, G. (1989), *Theory and Applications of Optical Remote Sensing*, Wiley-Interscience, New York.

BORIS (1993), BOREAS Information System, Goddard Space Flight Center, Greenbelt, MD.

Chen, J. (1996), Canopy architecture and remote sensing of the fraction of photosynthetically active radiation absorbed by boreal conifer forests. *IEEE Trans. Geosci. Remote Sens.* 34:1353–1367.

Chen, J., and Cihlar, J. (1996), Retrieval leaf area index of boreal

conifer forests using Landsat TM images. *Remote Sens. Environ.* 55:153–162.

Chen, J., and Leblanc, S. G. (1997), A four-scale bidirectional reflectance model based on canopy architecture. *IEEE Trans. Geosci. Remote Sens.* 35:1316–1337.

Chen, J., Rich, P. M., Gower, S. T., Norman, J. M., and Plummer, S. (1997), Leaf area index of boreal forests: theory, techniques, and measurements. *J. Geophys. Res.* 102:29,429–29,443.

Chen, J., Leblanc, S. G., Miller, J. R., et al. (1999), Compact Airborne Spectrographic Imager (CASI) used for mapping biophysical parameters of boreal forests. *J. Geophys. Res.* 104 (D22):27,945–27,958.

Gemmell, F., and Varjo, J. (1999), Utility of reflectance model inversion versus two spectral indices for estimating biophysical characteristics in a boreal forest test site. *Remote Sens. Environ.* 68:95–111.

Goel, N. S. (1988), Models of vegetation canopy reflectance and their use in estimation of biophysical parameters from reflectance data. *Remote Sens. Rev.* 4:1–212.

Gray, L., Freemantle, J., Shepherd, P., Miller, J., Harron, J., and Hersom, C. (1997), Characterization and calibration of the CASI airborne imaging spectrometer for BOREAS. *Can. J. Remote Sens.* 23:188–195.

Hall, F. G., Shimabukuro, Y. E., and Huemmrich, K. F. (1995), Remote sensing of forest biophysical structure using mixture decomposition and geometric reflectance model. *Ecol. Appl.* 5:993–1013.

Leblanc, S., Bicheron, P.,Chen, J. M., Leroy, M., and Cihlar, J. (1999), Investigation of directional reflectance in boreal forests with an improved four-scale model and airborne POLDER data. *IEEE Trans. Geosci. Remote Sens.* 37:1396–1414.

Leochel, S. E., Walthall, C. L., Brown de Colstoun, E., Chen, J., Markham, B. L., and Miller, J. (1997), Variability of boreal forest reflectances as measured from a helicopter platform. *J. Geophys. Res.* 102:29,495–29,503.

Li, X., and Strahler, A. H. (1988), Modeling the gap probability of a discontinuous vegetation canopy. *IEEE Trans. Geosci. Remote Sens.* 26:161–169.

Li, X., and Strahler, A. H. (1992), Geometric-optical bidirectional reflectance modeling of the discrete crown vegetation canopy: effect of crown shape and mutual shadowing. *IEEE Trans. Geosci. Remote Sens.* 30:276–291.

Li, X., Strahler, A. H., and Woodcock, C. E. (1995), A hybrid geometric optical-radiative transfer approach for modeling albedo and directional reflectance of discontinuous canopies. *IEEE Trans. Geosci. Remote Sens.* 33:466–480.

Miller, J. R., Freemantle, J., Shepherd, P., et al. (1995), Development of CASI to meet the needs of BOREAS science. In *Proceedings of the 17th Canadian Symposium on Remote Sensing*, Saskatoon, Saskatchewan, 13–15 June, pp. 169–175.

Miller, J. R., White, H. P., Chen, J. M., et al. (1997), Seasonal change in understory reflectance of boreal forests and influence on canopy vegetatiob indices. *J. Geophys. Res.* 102: 29,475–29,482.

Nilson, T., and Ross, J. (1997), Modeling radiative transfer through forest canopies: implications for canopy photosynthesis and remote sensing. In *The Use of Remote Sensing in the Modeling of Forest Productivity* (H. L. Gholz, K. Nakane, and H. Shimoda, Eds.), Kluwer Academic, Dordrecht.

O'Neill, N. T., Zagolski, F., Bergeron, M., Royer, A., Miller, J., and Freemantle, J. (1997), Atmospheric correction of CASI images acquired over the BORES southern study area. *Can. J. Remote Sens.* 23:143–162.

Rosema, A. W., Verhoef, W., Noorbergen, H., and Borgesius, J. J. (1992), A new forest light interaction model in support of forest monitoring. *Remote Sens. Environ.* 42:23–41.

Soffer, R., Miller, J. R., Wanner, W., and Strahler, A. H. (1995), Winter forest BRF results: comparisons between airborne data, laboratory simulations and geometrical-optical model data. In *Proceedings of the 1995 IEEE International Geoscience and Remote Sensing Symposium*, 10–14 July, Firenze, Italy, Vol. 1, pp. 800–805.

Verhoef, W. (1984), Light scattering by leaf layers with application to canopy reflectance modeling: the SAIL model. *Remote Sens. Environ.* 16:125–141.

Woodcock, C. E., Collins, J. B., Jakabhazy, V. D., Li, X., Macomber, S. A., and Wu, Y. (1997), Inversion of the Li and Strahler canopy reflectance model for mapping forest structure. *IEEE Trans. Geosci. Remote Sens.* 35:405–414.